THE JOURNAL OF PHYSICAL CHEMISTRY C

Article

pubs.acs.org/JPCC

Magnetic Coupling and Single-Ion Anisotropy in Surface-Supported Mn-Based Metal−Organic Networks

L. Giovanelli,*[,†] A. Savoyant,[†] M. Abel,[†] F. Maccherozzi,[‡] Y. Ksari,[†] M. Koudia,[†] R. Hayn,[†] F. Choueikani,[¶] E. Otero,[¶] P. Ohresser,[¶] J.-M. Themlin,[†] S. S. Dhesi,[‡] and S. Clair[†]

[†]Aix-Marseille Université, CNRS, IM2NP UMR 7334, F-13397 Marseille, France

[‡]Diamond Light Source, Didcot, OX11 0DE, United Kingdom

[¶]Synchrotron SOLEIL, L'orme des Merisiers, Saint-Aubin - BP48, 91192 Gif-sur-Yvette CEDEX, France

Supporting Information

ABSTRACT: The electronic and magnetic properties of Mn coordinated to 1,2,4,5-tetracyanobenzene (TCNB) in Mn−TCNB two-dimensional metal−ligand networks have been investigated by combining scanning tunneling microscopy and X-ray magnetic circular dichroism (XMCD) performed at low temperature (3 K). When formed on Au(111) and Ag(111) substrates, the Mn−TCNB networks display similar geometric structures. Magnetization curves reveal ferromagnetic coupling of the Mn sites with similar single-ion anisotropy energies but different coupling constants. Low-temperature XMCD spectra show that the local environment of the Mn centers differs appreciably for the two substrates. Multiplet structure calculations were used to derive the corresponding ligand field parameters, confirming an in-plane uniaxial anisotropy. The observed interatomic coupling is discussed in terms of superexchange as well as substrate-mediated magnetic interactions.

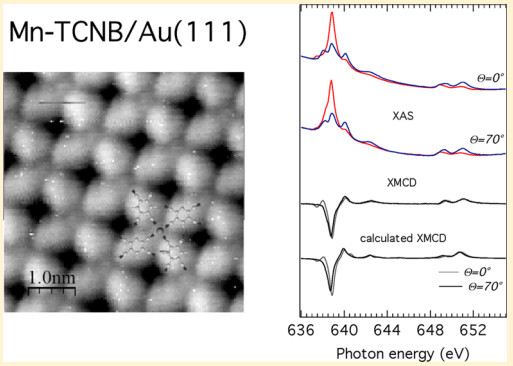

INTRODUCTION

Exploiting the functionality of organic molecules to manipulate electron spin has been the subject of intense scientific activity over the past few years.[1−3] The discovery of single-molecule magnets displaying high blocking temperatures and quantum tunneling of magnetization suggested an alternative method of downsizing information storage.[1,4−7] At the same time, low-Z organic materials showed high spin-transport coherence properties, making possible the integration of the spin degree of freedom in organics-based semiconductor devices.[2,8] For both aspects, the interface between the magnetically active constituents has been shown to have a crucial impact.[9−15]

Organic magnets were first reported for large-spin molecules such as Mn_{12}-ac.[16] More recently the use of smaller, π-conjugated macrocycles such as phthalocyanines and porphyrins hosting a single transition-metal atom has shown great versatility.[9,13−15,17] This includes, for instance, the possibility of modifying the magnetic spin state of the central metal atom through ferromagnetic (FM) coupling to the substrate[13,14,18] or by further adsorption of smaller molecules.[19,20] π-conjugated molecules are robust and can incorporate any transition metal. On the other hand they tend to organize via weak intermolecular bonding (van der Waals or H-bonding), thus limiting the possibility of designing new architectures at the nanoscale.

Currently an alternative approach for the synthesis of magneto-organic nanostructures is being explored. It consists of manipulating the magnetic properties of transition-metal atoms through selective bonding to functional ligands in surface-supported, self-assembled metal−organic networks.[3,21,22] Recent studies have shown that the magnetic coupling between metal centers, as well as their magnetic anisotropy, can be controlled by changing the nature of the metal−ligand (M-L) bonding or by adsorption of molecular oxygen.[3,21,22]

Significantly, two recent studies have revealed FM coupling between magnetic centers in two-dimensional (2D) organic self-assembled M-L networks.[21,22] In both cases a superexchange coupling was suggested. For Fe-T4PT/Au(111), spin-density oscillations across ligands propagated through the network.[21,23] In the case of Ni-TCNQ, the measured FM coupling for adsorption on Au(111) is ascribed to favorable M-L charge transfer, whereas for Ag(100) the participation of the substrate in the M-L interaction quenches the long-range order.[22]

In this context, the present study on the electronic structure and magnetic properties of a new M-L network, namely Mn coordinated with 1,2,4,5-tetracyanobenzene (Mn−TCNB) should bring a new piece of information for a comprehensive

Received: March 4, 2014
Revised: May 12, 2014
Published: May 12, 2014

   dx.doi.org/10.1021/jp502209q | J. Phys. Chem. C 2014, 118, 11738−11744

understanding of magnetic phenomena in organic M-L networks.

TCNB has raised interest recently for its potential ability to undergo a chemical reaction and form phthalocyanine derivatives or polymeric phthalocyanine.[24,25] The choice of the Mn is also important in view of total spin and magnetic anisotropy properties. A large anisotropy is necessary for magnetic memory applications, whereas small values open the way to qubit manipulation.[26] Mn with five d-electrons is a preferred candidate as a spin center in M-L networks. Under the action of organic ligands, the presence of intramolecular exchange interaction and sizable single-ion anisotropy were found,[27−29] making Mn-based organic molecules suitable for single-molecule magnetism. Recently, detailed structural and electronic studies on Mn-based M-L networks have been reported showing a rich interplay between metal centers, ligands, and different substrates,[30,31] suggesting the possibility of finely tuning the Mn magnetic properties.

In the present paper, scanning tunneling microscopy (STM) was used to study the structure of the Mn−TCNB M-L network grown on two different substrates, namely, Au(111) and Ag(111). Chemically and magnetically sensitive X-ray magnetic circular dichroism (XMCD[32]) in combination with spin Hamiltonian and multiplet calculations was used to study the effect of the M-L bonding on the Mn magnetic properties. A useful expression is also derived for the magnetic anisotropy energy of a d^5 configuration in a D_{4h} environment as a function of crystal field parameters.

EXPERIMENT

The experiments were performed at the DEIMOS beamline,[33] SOLEIL, France: it is an undulator beamline working in the soft-ray range with variable polarization. The end station houses a UHV sample preparation facility comprising sputtering and annealing for substrate preparation, molecular sublimation, STM, and Auger electron spectroscopy (AES). Au(111) and Ag(111) surfaces were prepared by repeated cycles of sputtering and annealing. Subsequently a single layer of TCNB was deposited by sublimating the molecules from a crucible while keeping the substrate at room temperature. Finally, additional sublimation of Mn atoms resulted in the formation of the Mn−TCNB M-L network domains with a given stoichiometry. The Au(111) sample was postannealed at 100 °C for 10 min to increase the homogeneity of the network. Every step of the procedure was monitored by STM and AES. The STM images of Figure 1 were obtained at IM2NP in Marseille in equivalent experimental conditions.

X-ray absorption spectroscopy (XAS) with variable polarization was performed in total electron yield mode. XMCD is the difference between XAS spectra acquired with circularly polarized light, with opposite alignment of X-ray helicity vector (99% circularly polarized light) and sample magnetization. The spectra were taken at 3 K and under a magnetic field of 6 T applied along the light propagation direction. Measurements were performed at normal incidence (NI; $\Theta = 0°$, Θ being the angle between the surface normal and the light beam) and at grazing incidence (GI; $\Theta = 70°$). XMCD was also used to record magnetization curves by scanning the magnetic field and measuring the difference between resonance and off-resonance XAS at each step. The signal was then normalized to the XAS signal at the highest applied magnetic field. The final curves are the average of four magnetic field scans performed after changing either the X-ray helicity or the magnetic field. All the magnetization curves have been normalized for comparison with a model Brillouin function. A least squares fit to mean field theory spin Hamiltonian containing zero-field splitting and FM coupling terms was performed.

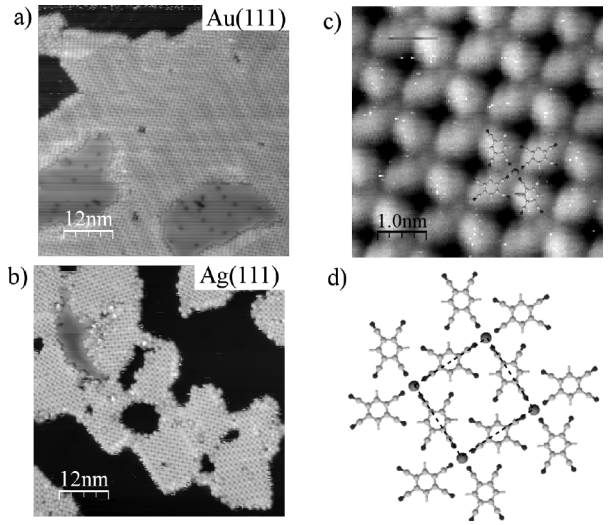

Figure 1. STM images of Mn−TCNB networks formed after deposition on (a) Au(111) and (b) Ag(111). (c) High-magnification image of the metal−organic structure on Au(111). (d) Ball−stick model showing the square unit cell (dashed line) of the network with a Mn/TCNB stoichiometry of 1:2.

SPIN HAMILTONIAN

A spin Hamiltonian with zero-field splitting (parameter D) and magnetic coupling between individual spins was used to fit the magnetization curves. This was done in the framework of mean field theory, where the magnetic interaction of a spin with all other spins is replaced by an effective mean magnetic field $\mathbf{B}_{eff}$ added to the external applied field $\mathbf{B}_{ext}$ and proportional to the mean magnetization $\mathbf{S}$.

$$H_S = DS_z^2 - g\mu_B \mathbf{B}\cdot\mathbf{S} \quad (1)$$

where $\mathbf{B} = \mathbf{B}_{ext} + \mathbf{B}_{eff}$ and $\mathbf{B}_{eff} = \lambda\mathbf{S}$. The Curie temperature associated with the magnetic coupling is given by $T_c = \lambda S(S+1)g\mu_B/(3k_B)$.[34] The strength of the coupling is related to the Curie temperature as $T_c = \sum J_i/(3k_B)$, where the sum goes over the first 4 neighboring sites of the square Mn-lattice. In fact, the magnetic field includes also a contribution of the local field created by dipolar interaction of all surrounding spins:

$$\mathbf{B} = \mathbf{B}_{ext} + \mathbf{B}_{eff} + \mathbf{B}_{dipol} \quad (2)$$

For an infinite 2D square spin−lattice of size a_0, $\mathbf{B}_{dipol}$ is of the order of $(8\pi/3a_0^3)g\mu_B\mathbf{S}$[35] and is about 1 order of magnitude smaller than the effective field $\mathbf{B}_{eff}$ due to magnetic interaction. Note that both zero-field splitting and magnetic interaction terms are necessary to obtain a reasonable fit to the experimental data.

MULTIPLET CALCULATIONS

The XMCD spectra were calculated in the framework of the ligand field multiplet. A numerical code was developed which diagonalized the microscopic Hamiltonian in the initial ($2p^63d^5$) and final ($2p^53d^6$) configurations[36] and then computed the dipole transitions. The microscopic Hamiltonian of the p and d many-electron system

dx.doi.org/10.1021/jp502209q | J. Phys. Chem. C 2014, 118, 11738−11744

$$H = H_C + H_{SO} + H_{LF} + H_Z \quad (3)$$

contains Coulomb repulsion in the d-shell and between p- and d-shells (H_C), spin−orbit interaction for p- and d-electrons (H_{SO}), ligand field (H_{LF}), and Zeeman interaction with an external magnetic field H_Z.

Considering a D_{4h} symmetry for the Mn^{2+} environment, the ligand field is defined by D_q, D_s, and D_t one-electron parameters. The last two give the deviation from a octahedral symmetry, characterized by $D_q > 0$.[38] The ligand field Hamiltonian defines the 4-fold z-axis. The external magnetic field is defined by its magnitude B and the θ angle it makes with the z-axis (within the (x,z) plane).

All these parameters being set, H is diagonalized in initial (252 states) and final (1260 states) configurations under saturating magnetic field, resulting in a set of eigenvalues and eigenvectors. Subsequently, the absorption spectra are calculated considering dipole-allowed transitions with circularly polarized light.[39] The resulting spectra are broadened by a Lorentzian function to take into account the finite lifetime of the core-hole.

RESULTS AND DISCUSSION

The STM images of Figure 1 show the Mn−TCNB networks formed after sequential deposition of TCNB and Mn. On Au(111), the domains are more extended (40 to 50 nm) than for Ag(111) (about 20 nm). The unit cell is square with a 1.2 ± 0.1 nm periodicity and comprises two molecules and one metal atom for both substrates, thus representing a $Mn(TCNB)_2$ stoichiometry. The corresponding schematic model of Figure 1d shows that each Mn atom is linked to 4 TCNB molecules through a Mn−N metal−ligand bonding displaying D_{4h} symmetry. The quality of the samples was assessed by in situ STM prior to XMCD measurements to confirm the formation of metal−organic domains.

In Figure 2, the XAS and XMCD spectra over the Mn $L_{3,2}$ edge are displayed for the two samples with the X-ray beam at different incidence angles. Despite the differences due to substrate background contributions, the overall shape of the XAS spectra are similar for the two systems: both exhibit the spectral features typical of Mn^{2+} with a d^5 configuration.[3,27−29,40−48] For both systems a clear difference is observed at the L_3 in going from NI to GI, indicating a preferred orbital orientation.

The XMCD also displays anisotropy for both systems, more markedly at the L_3. In NI, a negative−positive pre-edge is followed by a strong but featureless negative peak (at 638.9 and 639.0 eV for Au and Ag, respectively). In GI there is no clear pre-edge feature, but the main negative peak (638.8 and 638.9 eV for Au and Ag, respectively) has a shoulder at the low-energy side. Finally, the main peak intensity at GI is weaker than at NI. At the L_2 the differences are smaller, but it can be seen that the onset of the white line is shifted to lower energies in GI.

The XMCD spectra change significantly in going from Au(111) to Ag(111) substrate. The first difference is the quoted shift of 0.1 eV to higher energy for both sample orientations. The second, more clearly noticeable aspect is that on Ag(111) the shoulder at the main negative peak in GI is more pronounced than on Au(111) and the GI-to-NI difference of peak height is more marked. Finally the onset shift at the L_2 is larger for Ag(111).

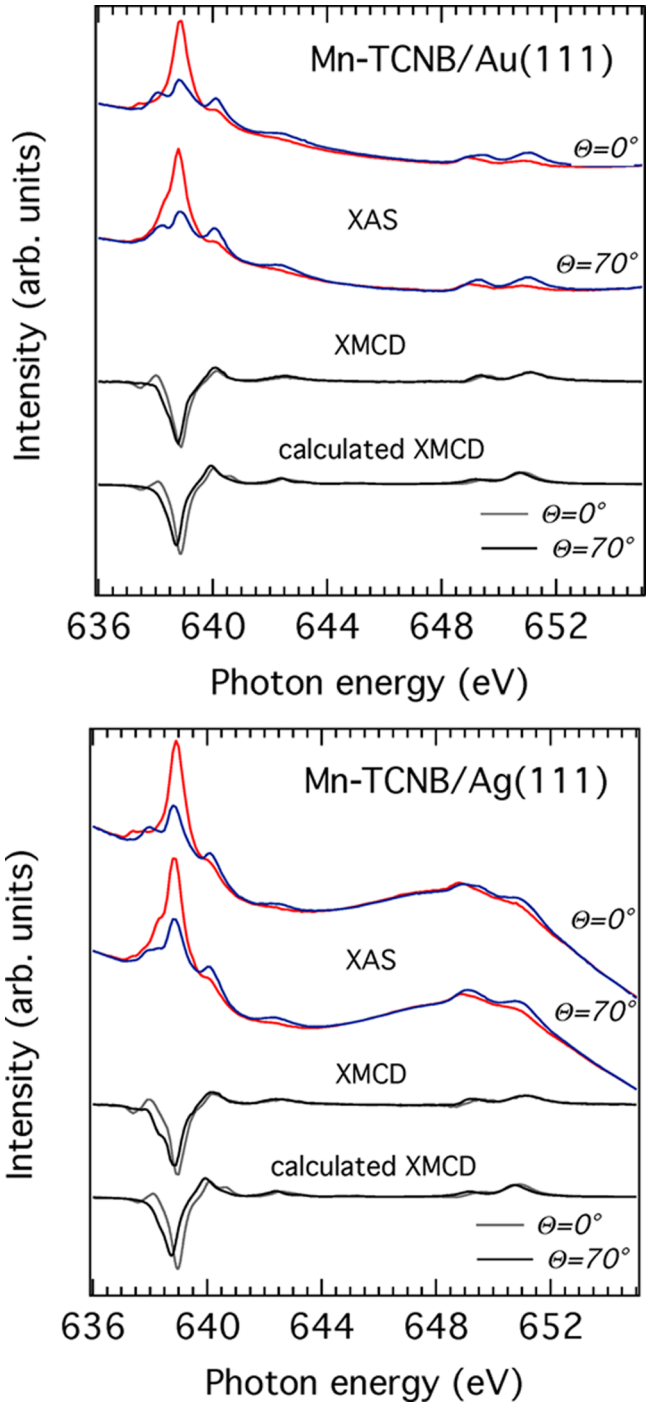

Figure 2. Angular dependence of the XAS and resulting XMCD over the Mn $L_{2,3}$ edge for (a) Mn−TCNB/Au(111) and (b) Mn−TCNB/Ag(111) measured at 3 K with an applied magnetic field of 6 T parallel (blue, dark) and antiparallel (red, light) to the X-ray beam helicity. Two sample orientations with respect to the light propagation direction were measured (Θ = 0° corresponds to normal incidence (NI) and Θ = 70° to grazing incidence (GI)). The bottom curves are obtained by ligand field multiplet calculations (see text). A normalization factor of 1.4 and 2.0 was applied to the calculated XMCD for Au(111) and Ag(111), respectively.

The magnetization curves for the two systems probed along the surface normal (NI) and close to sample surface plane (GI) are displayed in Figure 3. For Mn−TCNB/Au(111), a small in-plane magnetic anisotropy is detected. Both curves are close to

dx.doi.org/10.1021/jp502209q | J. Phys. Chem. C 2014, 118, 11738−11744

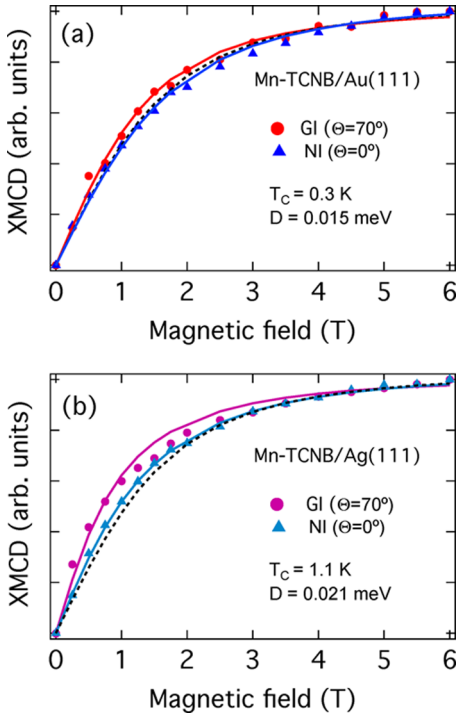

Figure 3. Magnetization curves (symbols) as obtained from XMCD of (a) Mn−TCNB/Au(111) and (b) Mn−TCNB/Ag(111) at 3 K in NI and GI geometries. Superimposed (continuous lines) are the least-squares fitting curves obtained through (eq 1) (see text for details). The resulting fitting parameters for the two systems are indicated. The Brillouin function at 3 K is shown for comparison as a dashed line.

the Brillouin function for a $S = 5/2$ system at 3 K. The same kind of anisotropy is measured for Mn−TCNB adsorbed on Ag(111). Remarkably, for Ag(111) a clear departure from the Brillouin function is observed, suggesting a FM coupling.[21,22] The anisotropy observed for both systems indicates an easy plane parallel to the network plane.

To gain more insight into the physical parameters governing the shape of the measured curves, we used a spin Hamiltonian with zero-field splitting (parameter D) and magnetic coupling between individual spins described above. The experimental curves were fitted by this model, and the following parameters were found (see Supporting Information for details): $D = 0.015$ meV and $T_c = 0.3$ K ($J_i = 0.02$ meV) for Au(111); $D = 0.021$ meV and $T_c = 1.1$ K ($J_i = 0.07$ meV) for Ag(111). The sign of the anisotropy parameter indicates an easy-plane uniaxial anisotropy for both systems. The anisotropy energy is similar and the coupling is sensibly stronger for the Ag(111) substrate.

The zero-field splitting (or single-ion anisotropy) energy results from the combined effect of the ligand field acting on the Mn atoms and the atomic d−d spin−orbit interaction. Because these parameters affect the XMCD, their approximate values can be inferred by comparing the experiment to parameter-dependent model spectra. XMCD spectra with varying ligand field parameters were therefore calculated. The best agreement was obtained when $10D_q = 0.7$ eV and $D_t = 0.07$ eV for both substrates and $D_s = 0.07$ eV and $D_s = 0.10$ eV for Au(111) and Ag(111), respectively.[49] The calculated spectra are displayed in the bottom parts of Figure 2a,b. All main experimental features are well-reproduced in terms of energy and relative intensity. Namely, the negative−positive pre-edge is present in the NI but absent in GI where a single negative peak is found instead. When Au(111) is changed to Ag(111), a higher D_s is found. This has several effects on the simulated spectra: (i) in GI a shoulder to the main negative peak develops at low energy; (ii) the difference in intensity at the main peak between GI and NI increases; and (iii) at the L_2 the onset shift becomes larger. All these features allow the correct reproduction of the main differences between the experimental spectra relative to Au and Ag substrates.

Despite the very good line shape agreement, the experimental XMCD is sensibly smaller than expected (a normalization factor of 1.4 and 2.0 was applied to the calculated XMCD for Au(111) and Ag(111), respectively). Similar reductions were found in other studies of Mn impurities on surfaces.[50,51] On Ge and GaAs, that was ascribed to a reduction of the spin moment because of hybridization of Mn d electrons with substrate states. Such hybridization can be ruled out in the present case because the XMCD spectral shape does not show the expected broadening.[50] When deposited on FM substrates, sub-ML quantities of Mn show a reduced XMCD because of the Mn−Mn bond formation resulting in d−d overlap and consequent antiferromagnetic (AFM) coupling.[51] In the present case it is indeed possible that part of the Mn atoms are engaged in AFM coupling, thus reducing the relative intensity of the XMCD signal. Another possible explanation may reside in the interaction of Mn d-states with delocalized substrate s-electrons. Such coupling was recently proposed to explain a quenching of the magnetic moment in CoPc/Au(111).[9] This scenario is indeed appealing but needs to be studied by interface charge-transfer multiplet calculation, an approach that is beyond the scope of the present paper.

Even without such refinements the ligand field parameter sets can be used to calculate D by means of the microscopic Hamiltonian. This was done analytically by exactly solving the Coulomb operator H_C in the initial configuration ($\equiv d^5$) and then treating H_{SO} and H_{LF} as perturbations to the ground sextet (^6S) energy. The result is a splitting of this sextet into three pseudospin doublets ($|\tilde{m}_S\rangle = |\pm\widetilde{5/2}\rangle, |\pm\widetilde{3/2}\rangle, |\pm\widetilde{1/2}\rangle$ from highest- to lowest-lying) separated by $4D$ and $2D$, respectively. Similar to the case of Mn^{2+} in C_{3v} symmetry,[52] the fourth-order expression of axial anisotropy for a d^5 configuration in D_{4h} symmetry is derived.[53]

$$D^{(4)} = \frac{63}{10}\frac{\zeta_d^2 D_s}{\mathcal{P}^2\mathcal{D}}\left(\zeta_d - \frac{D_s}{3}\right) + 35\frac{\zeta_d^2 D_t}{\mathcal{P}^2\mathcal{G}}(2D_q - D_t) \quad (4)$$

where $\mathcal{P} = 7(\mathcal{B} + C)$, $\mathcal{D} = 17\mathcal{B} + 5C$, and $\mathcal{G} = 10\mathcal{B} + 5C$ are, respectively, the energy difference between the ground state sextet ^6S and excited quartets of the d^5 configuration lying just above in energy: ^4G, ^4P, and ^4D. $\mathcal{B}$ and C are the Racah parameters, related to the Slater−Condon's by $F^2_{dd} = 49\mathcal{B} + 7C$ and $F^4_{dd} = 63C/5$.[54] This formula relates one-electron ligand field (electric field plus hybridization) anisotropy parameters (D_q, D_t and D_s) to the magnetic anisotropy parameter (D) of a $S = 5/2$. Equation 4 is thus very important for predicting the effect of a modified chemical environment on the magnetic anisotropy properties.

When using $\zeta_d = 0.052$ eV, the resulting value of D is 0.012 and 0.011 meV for Au and Ag, respectively. Such values are somehow smaller than those obtained by fitting the magnetization curves (for Au and Ag 0.015 and 0.021 meV, respectively). Nevertheless they confirm the presence of the single ion, easy-plane, uniaxial anisotropy.[55] Moreover, from eq 4 it results that although the in-plane tetragonal distortion D_s

dx.doi.org/10.1021/jp502209q | J. Phys. Chem. C 2014, 118, 11738−11744

affects the angular dependence of the XMCD spectrum (of course in combination with D_t), it has only a weak influence on the anisotropy energy which is determined mainly by D_q and D_t through the spin−orbit interaction and is therefore very similar for the two substrates.

The results reported above indicate that within the Mn−TCNB M-L network, magnetic anisotropy is induced by the joint effect of ligand field and spin−orbit interaction. Comparatively, the zero-field splitting reported recently for high-spin, d^5 Mn in a star-shaped heteronuclear complex ($Cr^{III}Mn^{II}_3$) is as high as 0.124 meV.[28] On the other hand, the magnetic coupling constant found here is higher than that reported for star-shaped molecules having a shorter Mn−Mn distance.[28,29] This may be due to the extended two-dimensional character of the present system and to the presence of the metallic substrate, favoring delocalization of magnetic excitations.

Concerning the mechanism driving the magnetic coupling, previous FM behavior on 2D organic M-L networks was ascribed to superexchange interaction.[21,22] Superexchange may also be the driving interaction in the case of Mn−TCNB. In such a perspective it should be noted that for the Ag-supported system the D_s obtained from the XMCD simulation is higher than that for Au. This may arise from a more effective M-L linkage resulting in a stronger magnetic coupling.

However, the coupling mechanisms suggested in the previous studies of organic M-L networks are probably not adapted for explaining the behavior encountered here. In fact, for Mn−TCNB, the number of linker atoms between each Mn is even; thus, a superexchange interaction through spin density oscillation should be AFM.[23] A charge-state-dependent coupling as observed for Ni-TCNQ[22] is not observed for Mn−TCNB where XAS spectra reveal that the charge state of the Mn atoms is the same on both substrates.

Conversely, for the present systems, a substrate-mediated FM coupling can be envisaged through Ruderman−Kittel−Kasuya−Yosida (RKKY) interactions.[56] In fact, above (111) noble metal surfaces collective screening occurs through the Schockley state, and to a first approximation, the key parameter determining the sign of the exchange interaction is the product of the lattice constant and the Fermi wave vector (k_F). Using the expression for RKKY interactions in 2D,[57] one observes that the relatively small k_F of Ag(111) favors FM coupling between nearest neighbors (placed 1.2 nm apart). On the other hand, for Au(111) the two Rashba-split Schockley states have larger k_F values, and at a distance of 1.2 nm, the first minimum for the RKKY interaction is reached, resulting in a moderate AFM coupling. Certainly the real situation is more complex than the above scenario. Nevertheless, in a picture in which RKKY would compete with other channels of magnetic coupling (such as superexchange as mentioned earlier), the FM-to-AFM screening in going from Ag(111) to Au(111) may help to explain the differences measured in the magnetization curves of the two otherwise very similar Mn−TCNB networks. It would be interesting to test such a scenario for Ag(100) substrate where the surface states are unoccupied and no long-range oscillation of the exchange interactions is expected.[58]

CONCLUSION

In summary, the structure and the magnetic properties of two Mn−TCNB metal−ligand networks were studied by STM and low-temperature XMCD. Angle-dependent magnetization curves show FM coupling between the equally spaced Mn atoms with in-plane uniaxial anisotropy. Ligand field multiplet calculations were used to simulate the experimental spectra. The obtained parameter values allow an estimation of the anisotropy energy, confirming the magnetization curve analysis. The spectroscopic differences between Mn−TCNB on Au(111) and Ag(111) indicate a stronger in-plane distortion of the ligand field for adsorption on Ag(111). This may be the result of a stronger metal−ligand interaction favoring superexchange coupling. Another possible explanation for the different magnetic coupling between Ag(111) and Au(111) is given in terms of RKKY interaction. Because M-L networks are versatile extended 2D systems in which the interatomic distance is controlled by the choice of the organic linkers, in the future they may emerge as a new approach to the study of surface magnetic screening phenomena beside single-atom manipulation[59] and self-assembly of π-conjugated molecules containing magnetic centers.[56] Finally, an expression (eq 4) is given for the magnetic anisotropy energy of a d^5 configuration in a D_{4h} environment as a function of crystal field parameters. This should be seen as a helpful tool to predict, and possibly tune, the magnetic anisotropy properties via organic linkers. A future development of the model will focus on the magnetic coupling, possibly including hybridization and surface-mediated interactions.

ASSOCIATED CONTENT

Supporting Information

Details on the fitting procedure of the magnetization curves. This material is available free of charge via the Internet at http://pubs.acs.org.

AUTHOR INFORMATION

Corresponding Author

*E-mail: luca.giovanelli@im2np.fr.

Notes

The authors declare no competing financial interest.

ACKNOWLEDGMENTS

The preparation chambers of the DEIMOS beamline have been partially funded by the Agence National de la Recherche (Grant ANR-05-NANO-073).

REFERENCES

(1) Miyamachi, T.; Gruber, M.; Davesne, V.; Bowen, M.; Boukari, S.; Joly, L.; Scheurer, F.; Rogez, G.; Yamada, T. K.; Ohresser, P.; et al. Robust Spin Crossover and Memristance across a Single Molecule. *Nat. Commun.* **2012**, *3*, 1.

(2) Sanvito, S. Molecular Spintronics. *Chem. Soc. Rev.* **2011**, *40*, 3336.

(3) Gambardella, P.; Stepanow, S.; Dmitriev, A.; Honolka, J.; de Groot, F. M. F.; Lingenfelder, M.; Gupta, S. S.; Sarma, D. D.; Bencok, P.; Stanescu, S.; et al. Supramolecular Control of the Magnetic Anisotropy in Two-dimensional High-Spin Fe Arrays at a Metal Interface. *Nat. Mater.* **2009**, *8*, 189.

(4) Ghigna, P.; Campana, A.; Lascialfari, A.; Caneschi, A.; Gatteschi, D.; Tagliaferri, A.; Borgatti, F. X-ray Magnetic-circular-dichroism Spectra on the Superparamagnetic Transition-Metal Ion Clusters Mn12 and Fe8. *Phys. Rev. B* **2001**, *64*, 132413.

(5) Schlegel, C.; van Slageren, J.; Manoli, M.; Brechin, E. K.; Dressel, M. Direct Observation of Quantum Coherence in Single-Molecule Magnets. *Phys. Rev. Lett.* **2008**, *101*, 147203.

(6) Mannini, M.; Pineider, F.; Sainctavit, P.; Danieli, C.; Otero, E.; Sciancalepore, C.; Talarico, A. M.; Arrio, M.-A.; Cornia, A.; Gatteschi, D.; et al. Magnetic Memory of a Single-Molecule Quantum Magnet Wired to a Gold Surfaces. *Nat. Mater.* **2009**, *8*, 194.

(7) Stepanow, S.; Honolka, J.; Gambardella, P.; Vitali, L.; Abdurakhmanova, N.; Tseng, T.-C.; Rauschenbach, S.; Tait, S. L.; Sessi, V.; Klyatskaya, S.; et al. Spin and Orbital Magnetic Moment Anisotropies of Monodispersed Bis(phthalocyaninato)terbium on a Copper Surface. *J. Am. Chem. Soc.* **2010**, *132*, 11900.
(8) Raman, K. V.; Kamerbeek, A. M.; Mukherjee, A.; Atodiresei, N.; Sen, T. K.; Lazic, P.; Caciuc, V.; Michel, R.; Stalke, D.; Mandal, S. K.; et al. Interface-Engineered Templates for Molecular Spin Memory Devices. *Nature (London, U.K.)* **2013**, *493*, 509.
(9) Stepanow, S.; Miedema, P. S.; Mugarza, A.; Ceballos, G.; Moras, P.; Cezar, J. C.; Carbone, C.; de Groot, F. M. F.; Gambardella, P. Mixed-Valence Behavior and Strong Correlation Effects of Metal Phthalocyanines Adsorbed on Metals. *Phys. Rev. B* **2011**, *83*, 220401.
(10) Sanvito, S. The Rise of Spinterface Science. *Nat. Phys.* **2010**, *6*, 562.
(11) Javaid, S.; Bowen, M.; Boukari, S.; Joly, L.; Beaufrand, J.-B.; Chen, X.; Dappe, Y. J.; Scheurer, F.; Kappler, J.-P.; Arabski, J.; et al. Impact on Interface Spin Polarization of Molecular Bonding to Metallic Surfaces. *Phys. Rev. Lett.* **2010**, *105*, 077201.
(12) Wende, H.; Bernien, M.; Luo, J.; Sorg, C.; Ponpandian, N.; Kurde, J.; Miguel, J.; Piantek, M.; Xu, X.; Eckhold, P.; et al. Substrate-Induced Magnetic Ordering and Switching of Iron Porphyrin Molecules. *Nat. Mater.* **2007**, *6*, 516.
(13) Annese, E.; Fujii, J.; Vobornik, I.; Panaccione, G.; Rossi, G. Control of the Magnetism of Cobalt Phthalocyanine by a Ferromagnetic Substrate. *Phys. Rev. B* **2011**, *84*, 174443.
(14) Annese, E.; Casolari, F.; Fujii, J.; Rossi, G. Interface Magnetic Coupling of Fe-phthalocyanine Layers on a Ferromagnetic Surface. *Phys. Rev. B* **2013**, *87*, 054420.
(15) Gargiani, P.; Rossi, G.; Biagi, R.; Corradini, V.; Pedio, M.; Fortuna, S.; Calzolari, A.; Fabris, S.; Cezar, J. C.; Brookes, N. B.; et al. Spin and Orbital Configuration of Metal Phthalocyanine Chains Assembled on the Au(110) Surface. *Phys. Rev. B* **2013**, *87*, 165407.
(16) Thomas, L.; Lionti, F.; Ballou, R.; Gatteschi, D.; Sessoli, R.; Barbara, B. Macroscopic Quantum Tunnelling of Magnetization in a Single Crystal of Nanomagnets. *Nature (London, U.K.)* **1996**, *383*, 145.
(17) Stepanow, S.; Mugarza, A.; Ceballos, G.; Moras, P.; Cezar, J. C.; Carbone, C.; Gambardella, P. Giant Spin and Orbital Moment Anisotropies of a Cu-Phthalocyanine Monolayer. *Phys. Rev. B* **2010**, *82*, 014405.
(18) Bernien, M.; Miguel, J.; Weis, C.; Ali, M. E.; Kurde, J.; Krumme, B.; Panchmatia, P. M.; Sanyal, B.; Piantek, M.; Srivastava, P.; et al. Tailoring the Nature of Magnetic Coupling of Fe-Porphyrin Molecules to Ferromagnetic Substrates. *Phys. Rev. Lett.* **2009**, *102*, 047202.
(19) Wäckerlin, C.; Chylarecka, D.; Kleibert, A.; Müller, K.; Iacovita, C.; Nolting, F.; Jung, T. A.; Ballav, N. Controlling Spins in Adsorbed Molecules by a Chemical Switch. *Nat. Commun.* **2010**, *1*, 61.
(20) Isvoranu, C.; Wang, B.; Schulte, K.; Ataman, E.; Knudsen, J.; Andersen, J. N.; Bocquet, M. L.; Schnadt, J. Tuning the Spin State of Iron Phthalocyanine by Ligand Adsorption. *J. Phys.: Condens. Matter* **2010**, *22*, 472002.
(21) Umbach, T. R.; Bernien, M.; Hermanns, C. F.; Krüger, A.; Sessi, V.; Fernandez-Torrente, I.; Stoll, P.; Pascual, J. I.; Franke, K. J.; Kuch, W. Ferromagnetic Coupling of Mononuclear Fe Centers in a Self-Assembled Metal-Organic Network on Au(111). *Phys. Rev. Lett.* **2012**, *109*, 267207.
(22) Abdurakhmanova, N.; Tseng, T.-C.; Langner, A.; Kley, C. S.; Sessi, V.; Stepanow, S.; Kern, K. Superexchange-Mediated Ferromagnetic Coupling in Two-Dimensional Ni-TCNQ Networks on Metal Surfaces. *Phys. Rev. Lett.* **2013**, *110*, 027202.
(23) Bellini, V.; Lorusso, G.; Candini, A.; Wernsdorfer, W.; Faust, T. B.; Timco, G. A.; Winpenny, R. E. P.; Affronte, M. Propagation of Spin Information at the Supramolecular Scale through Heteroaromatic Linkers. *Phys. Rev. Lett.* **2011**, *106*, 227205.
(24) Abel, M.; Clair, S.; Ourdjini, O.; Mossoyan, M.; Porte, L. Single Layer of Polymeric Fe-Phthalocyanine: A Fully Conjugated Organometallic Sheet. *J. Am. Chem. Soc.* **2011**, *133*, 1203.
(25) Sedlovets, D. M.; Shuvalov, M. V.; Vishnevskiy, Y. V.; Volkov, V. T.; Khodos, I. I.; Trofimov, O. V.; Korepanov, V. I. Synthesis and Structure of High-Quality Films of Copper Polyphthalocyanine-2d Conductive Polymer. *Mater. Res. Bull.* **2013**, *48*, 3955.
(26) Bertaina, S.; Chen, L.; Groll, N.; Van Tol, J.; Dalal, N. S.; Chiorescu, I. Multiphoton Coherent Manipulation in Large-Spin Qubits. *Phys. Rev. Lett.* **2009**, *102*, 050501.
(27) Kuepper, K.; Benoit, D. M.; Wiedwald, U.; Mögele, F.; Meyering, A.; Neumann, M.; Kappler, J.-P.; Joly, L.; Weidle, S.; Rieger, B.; et al. Precise Chemical, Electronic, and Magnetic Structure of Binuclear Complexes Studied by Means of X-ray Spectroscopies and Theoretical Methods. *J. Phys. Chem. C* **2011**, *115*, 25030−25039.
(28) Prinz, M.; Kuepper, K.; Taubitz, C.; Raekers, M.; Khanra, S.; Biswas, B.; Weyhermüller, T.; Uhlarz, M.; Wosnitza, J.; Schnack, J.; et al. A Star-Shaped Heteronuclear $Cr^{III}Mn^{II}_3$ Species and Its Precise Electronic and Magnetic Structure: Spin Frustration Studied by X-ray Spectroscopic, Magnetic, and Theoretical Methods. *Inorg. Chem.* **2010**, *49*, 2093.
(29) Khanra, S.; Kuepper, K.; T. W; Prinz, M.; Raekers, M.; Voget, S.; Postnikov, A. V.; de Groot, F. M. F.; George, S. J.; Coldea, M.; et al. Star-Shaped Molecule of $Mn^{II}_4O_6$ Core with an S_t = 10 High-Spin State. A Theoretical and Experimental Study with XPS, XMCD, and Other Magnetic Methods. *Inorg. Chem.* **2008**, *47*, 4605−4617.
(30) Tseng, T.-C.; Lin, C.; Shi, X.; Tait, S. L.; Liu, X.; Starke, U.; Lin, N.; Zhang, R.; Minot, C.; Van Hove, M. A.; et al. Two-Dimensional Metal-Organic Coordination Networks of Mn-7,7,8,8-tetracyanoquinodimethane Assembled on Cu(100): Structural, Electronic, and Magnetic Properties. *Phys. Rev. B* **2009**, *80*, 155458.
(31) Faraggi, M. N.; Jiang, N.; Gonzalez-Lakunza, N.; Langner, A.; Stepanow, S.; Kern, K.; Arnau, A. Bonding and Charge Transfer in Metal−Organic Coordination Networks on Au(111) with Strong Acceptor Molecules. *J. Phys. Chem. C* **2012**, *116*, 24558.
(32) Stöhr, J. Exploring the Microscopic Origin of Magnetic Anisotropies with X-ray Magnetic Circular Dichroism (XMCD) Spectroscopy. *J. Magn. Magn. Mater.* **1999**, *200*, 470.
(33) Ohresser, P.; Otero, E.; Choueikani, F.; Chen, K.; Stanescu, S.; Deschamps, F.; Moreno, T.; Polack, F.; Lagarde, B.; Daguerre, J.-P.; et al. DEIMOS: A Beamline Dedicated to Dichroism Measurements in the 350−2500 eV Energy Range. *Rev. Sci. Instrum.* **2014**, *85*, 013106.
(34) Ashcroft, N. W.; Mermin, N. D. In *Solid State Physics*; Crane, D. G., Ed.; Harcourt: Orlando, FL, 1976.
(35) Yafet, Y.; Gyorgy, E. M. Ferromagnetic Strip Domains in an Atomic Monolayer. *Phys. Rev. B* **1988**, *38*, 9145−9151.
(36) The Hartree−Fock energies reduced to 80% of the atomic values as obtained from the CTM4XAS program[37] were used.
(37) Stavitski, E.; de Groot, F. M. The CTM4XAS Program for EELS and XAS Spectral Shape Analysis of Transition Metal L Edges. *Micron* **2010**, *41*, 687.
(38) De Groot, F. Multiplet Effects In X-ray Spectroscopy. *Coord. Chem. Rev.* **2005**, *249*, 31.
(39) Kuz'min, M. D.; Hayn, R.; Oison, V. Ab Initio Calculated Xanes and XMCD Spectra of Fe(II) Phthalocyanines. *Phys. Rev. B* **2009**, *79*, 024413.
(40) Arrio, M.-A.; Sainctavit, P.; Cartier dit Moulin, C.; Mallah, T.; Verdaguer, M.; Pellegrin, E.; Chen, C. T. Characterization of Chemical Bonds in Bimetallic Cyanides Using X-ray Absorption Spectroscopy at L2,3 Edges. *J. Am. Chem. Soc.* **1996**, *118*, 6422.
(41) Nanba, Y.; Okada, K. Theory of Fe and Mn 2*p* X-ray Absorption for $RbMn[Fe(CN)_6]$. *J. Electron Spectrosc. Relat. Phenom.* **2012**, *185*, 167.
(42) Gambardella, P.; Claude, L.; Rusponi, S.; Franke, K. J.; Brune, H.; Raabe, J.; Nolting, F.; Bencok, P.; Hanbicki, A. T.; Jonker, B. T.; et al. Surface Characterization of $MnxGe_{1-x}$ and $CryMn_xGe_{1-x-y}$ Dilute Magnetic Semiconductors. *Phys. Rev. B* **2007**, *75*, 125211.
(43) Nagel, M.; Biswas, I.; Nagel, P.; Pellegrin, E.; Schuppler, S.; Peisert, H.; Chassé, T. Ultrathin Transition-Metal Oxide Films: Thickness Dependence of the Electronic Structure and Local Geometry in MnO. *Phys. Rev. B* **2007**, *75*, 195426.
(44) Kang, J.-S.; Kim, G.; Lee, H. J.; Kim, D. H.; Kim, H. S.; Shim, J. H.; Lee, S.; Lee, H.; Kim, J.-Y.; Kim, B. H.; et al. Soft X-ray Absorption

Spectroscopy and Magnetic Circular Dichroism Study of the Valence and Spin States in Spinel $MnFe_2O_4$. *Phys. Rev. B* **2008**, *77*, 035121.
(45) Edmonds, K. W.; van der Laan, G.; Freeman, A. A.; Farley, N. R. S.; Johal, T. K.; Campion, R. P.; Foxon, C. T.; Gallagher, B. L.; Arenholz, E. Angle-Dependent X-ray Magnetic Circular Dichroism from (Ga,Mn)As: Anisotropy and Identification of Hybridized States. *Phys. Rev. Lett.* **2006**, *96*, 117207.
(46) Maccherozzi, F.; Sperl, M.; Panaccione, G.; Minár, J.; Polesya, S.; Ebert, H.; Wurstbauer, U.; Hochstrasser, M.; Rossi, G.; Woltersdorf, G.; et al. Evidence for a Magnetic Proximity Effect up to Room Temperature at Fe/(Ga,Mn)As Interfaces. *Phys. Rev. Lett.* **2008**, *101*, 267201.
(47) Cramer, S. P.; DeGroot, F. M. F.; Ma, Y.; Chen, C. T.; Sette, F.; Kipke, C. A.; Eichhorn, D. M.; Chan, M. K.; Armstrong, W. H.; et al. Ligand Field Strengths and Oxidation States From Manganese L-Edge Spectroscopy. *J. Am. Chem. Soc.* **1991**, *113*, 7937.
(48) de Groot, F. M. F.; Fuggle, J. C.; Thole, B. T.; Sawatzky, G. A. 2 *p* X-ray Absorption of 3 *d* Transition-Metal Compounds: An Atomic Multiplet Description Including the Crystal Field. *Phys. Rev. B* **1990**, *42*, 5459.
(49) To improve the fit, a reduction to 90% of the atomic value was applied to the p−d Coulomb interaction.
(50) Gambardella, P.; Brune, H.; Dhesi, S. S.; Bencok, P.; Krishnakumar, S. R.; Gardonio, S.; Veronese, M.; Grazioli, C.; Carbone, C. Paramagnetic Mn Impurities on Ge and GaAs Surfaces. *Phys. Rev. B* **2005**, *72*, 045337.
(51) Dürr, H. A.; van der Laan, G.; Spanke, D.; Hillebrecht, F. U.; Brookes, N. B. Electron-Correlation-Induced Magnetic Order of Ultrathin Mn Films. *Phys. Rev. B* **1997**, *56*, 8156.
(52) Savoyant, A.; Stepanov, A.; Kuzian, R.; Deparis, C.; Morhain, C.; Grasza, K. Single-Ion Anisotropy in Mn-Doped Diluted Magnetic Semiconductors. *Phys. Rev. B* **2009**, *80*, 115203.
(53) When calculating the energies of $H = DS_z^2$ for a spin 5/2 (six states), one finds 3 doublets separated by 2*D* and 4*D* (giving 6*D* between the lowest and the highest). The perturbative calculation of level ^6S gives exactly 3 doublets separated by the same ratio, which allows the assignment of them to those of an effective 5/2 spin under the action of $H = DS_z^2$. It should be noted that the expression for *D* is equally valid for the following symmetries: D_4, D_{2d} and C_{4v}.
(54) Unreduced values of $F_{dd}^2 = 8.253$ and $F_{dd}^4 = 5.131$ were used, as obtained from CTMX program.[37] A reduction of these parameters gives a higher *D* value through eq 4, but the fitting to the experimental curves is poorer.
(55) It has to be stressed that values of *D* closer to those obtained from fitting the magnetization curves can be obtained through eq 4 by further increasing the spin−orbit parameter ζ and without altering the simulated XMCD spectrum appreciably. Nevertheless, a free ion value was chosen because ζ is known to be *reduced* by the effect of the environment.
(56) Tsukahara, N.; Shiraki, S.; Itou, S.; Ohta, N.; Takagi, N.; Kawai, M. Evolution of Kondo Resonance from a Single Impurity Molecule to the Two-Dimensional Lattice. *Phys. Rev. Lett.* **2011**, *106*, 187201.
(57) Fischer, B.; Klein, M. W. Magnetic and Nonmagnetic Impurities in Two-Dimensional Metals. *Phys. Rev. B* **1975**, *11*, 2025.
(58) Simon, E.; Újfalussy, B.; Lazarovits, B.; Szilva, A.; Szunyogh, L.; Stocks, G. M. Exchange Interaction between Magnetic Adatoms on Surfaces of Noble Metals. *Phys. Rev. B* **2011**, *83*, 224416.
(59) Khajetoorians, A. A.; Wiebe, J.; Chilian, B.; Lounis, S.; Blugel, S.; Wiesendanger, R. Atom-by-Atom Engineering and Magnetometry of Tailored Nanomagnets. *Nat. Phys.* **2012**, *8*, 497.